



Analysis of the fatigue performance of elastic rail clip

Anat Hasap^a, Phanasindh Paitekul^a, Nitikorn Noraphaiphaksa^b,
Chaosuan Kanchanomai^{b,*}

^a Railway Transportation System Testing Centre (RTTC), Thailand Institute of Scientific and Technological Research, Pathumthani 12120, Thailand

^b Center of Materials Engineering and Performance (CMEP), Department of Mechanical Engineering, Faculty of Engineering, Thammasat University, Pathumthani 12120, Thailand



ARTICLE INFO

Keywords:

Elastic rail clip
Toe load
Wheel load
Fatigue

ABSTRACT

As a critical component of railway fastening system, the elastic rail clip (e-clip) maintains the rail position using its specified toe load. To understand its fatigue failure during service, the fatigue experiment, finite element analysis (FEA) and failure analysis were performed on e-clip. Under normal wheel load, e-clips with high, normal, and low toe loads were run-out at 5×10^6 cycles. Under the contribution of impact on wheel load, the fatigue lives were reduced to 5468 cycles and 16,839 cycles for e-clips with high and normal toe loads, respectively. For low toe load, the e-clip under the contribution of impact could withstand $> 5 \times 10^6$ cycles. The stress distribution on e-clip was numerically evaluated using FEA, which was in good agreement with that of experiment. Goodman diagram could be used for the fatigue evaluation of e-clip. The mean stresses and stress amplitudes of run-out e-clips were under the line of Goodman equation, while those of failed e-clips were on and above the line of Goodman equation. The fatigue crack was found to nucleate at the location of highest stress. The severity at fatigue crack front increased with the crack length until the overload fracture.

1. Introduction

In modern railway track system, various components, e.g., rail, pad, insulator, rail clip, base plate, form a complex fastening system [1,2]. One critical component of the fastening system is the rail clip, which applies compressive force (toe load) and maintains the rail in vertical, lateral and longitudinal positions. An important criterion to ensure proper function of the rail clip is the specified toe load during the installation. During operation, the rail clips are subjected to the combination between toe load (static load) and repeated wheel load (cyclic load), which can cause fatigue failure [3]. Moreover, the impact caused by irregularities of rail and wheel, e.g., weldment, wear, corrugated rail, can add up to 60% of the wheel load [4,5]. The increases in mean load (toe load) and cyclic load (wheel load and impact) enhance the cyclic deformation of rail clip, which accelerates the fatigue failure. It is therefore necessary to systematically investigate the influence of these loads on fatigue failure of rail clip.

Mohammadzadeh et al. [5] proposed a method for fatigue reliability analysis of the fastening spring clip under operating condition. The displacement-time history was applied to the finite element analysis (FEA) of fastening spring clip. The crack nucleation life was numerically estimated using rain-flow method and Palmgren-Miner linear damage rule. Unfortunately, the experimental and in-service fatigue lives were not compared with their results to verify the. Tamagawa et al. [6] developed a fatigue limit diagram for the “wire-shaped” clip, i.e., the relationship between the mean strain and the strain amplitude. Their fatigue life predictions using a fatigue limit diagram were in good agreement with those of fatigue tests. Sadeghi et al. [7] experimentally evaluated the influence of

* Corresponding author.

E-mail address: kchao@engr.tu.ac.th (C. Kanchanomai).

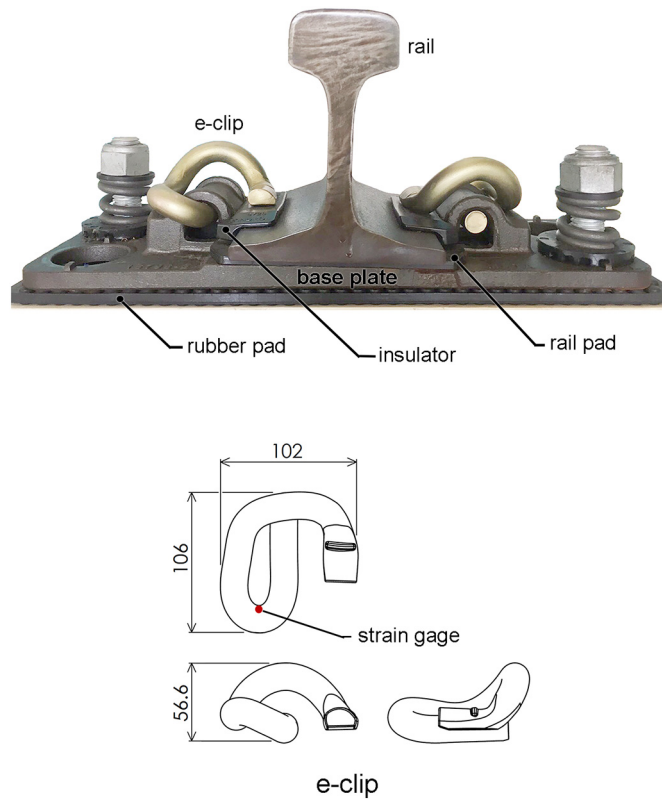


Fig. 1. (a) Railway track system, and (b) Geometry of elastic rail clip (dimension in mm).

the rail loading conditions on fatigue phenomena of Vossloh and Pandrol flexible clips under various train speeds and axle loads. The increases of axle loads caused substantial increases in the clip plastic deformations, while the train speeds had less influence on the deflection. A comparison of the results obtained for two types of e-clips (Vossloh and Pandrol) indicated that both railway flexible clips had the similar fatigue behavior. Shang et al. [8] numerically evaluated the effect of the vertical displacement of clip's finger on the clamping force and stress. The vertical displacement of clip's finger had marginal effect on the clamping force, but a large effect on the maximum equivalent stress in the clip. They suggested that the fatigue crack might easily nucleate and propagate in the clip's stress concentration area after repeated passages of trains.

Although there are literatures focused on the reliability of rail clips, the fatigue failure analysis of elastic rail clip, e.g., stress/strain distribution, fatigue life, crack nucleation, crack propagation, has not been clearly understood, especially for the elastic rail clip under the contribution of impact. In the present work, the fatigue experiments were performed on elastic rail clip, while the stress distribution on elastic rail clip has been determined using the finite element analysis (FEA). The fractured clip was observed under a stereomicroscope and a scanning electron microscope (SEM); then the failure mechanism has been discussed. The findings can be used as a guideline for the installation and maintenance of railway track system, and also applied to the improvement of an elastic rail clip.

2. Material and methods

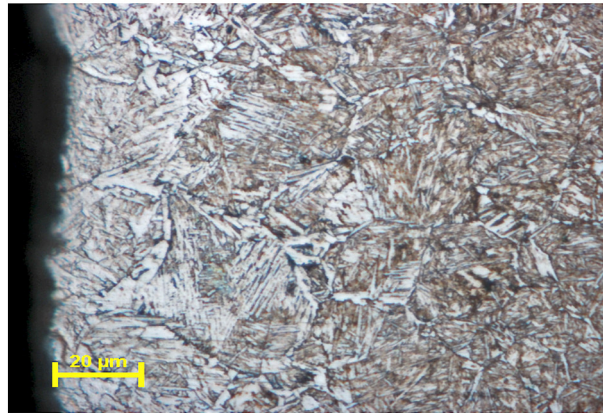
2.1. Elastic rail clip

In a fastening system, an elastic rail clip (e-clip) is clamped between the insulator and base plate with the rail and rail pad in the middle (Fig. 1). A rod of spring steel was machined, heated and coiled to obtain the geometry of e-clip (Fig. 1). Its chemical

Table 1
Chemical composition of e-clip (wt%).

Element	C	Si	Mn	Cr	Cu	Fe
e-clip	0.532	1.800	0.841	0.244	0.181	Bal.
Si-Cr spring steel [15]	0.56	1.44	0.68	0.70	0.01	Bal.
SUP7 spring steel [9]	0.55–0.65	1.80–2.20	0.70–1.00	–	< 0.30	Bal.

surface of cross section



center of cross section

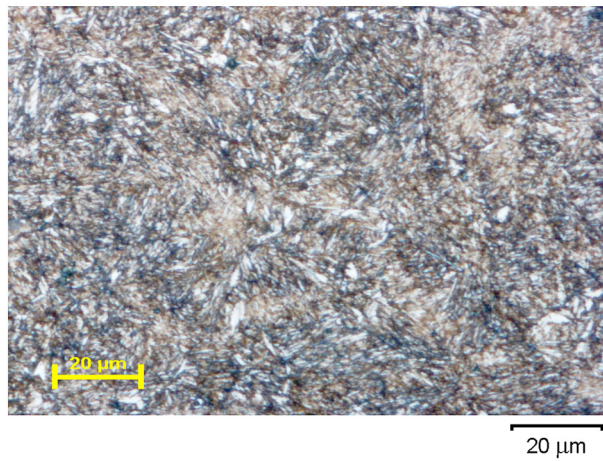


Fig. 2. Microstructure of elastic rail clip.

composition was evaluated using an emission spectrometer (Spectrolab: M10) in three locations, and the averages are listed in Table 1. The chemical composition of e-clip is closed to that of SUP7 spring steel recommended by JIS G4801 [9]. However, the weight percentages of C and Cr are slightly different than those of SUP7 spring steel.

At the location indicated by a dot on e-clip in Fig. 1, an e-clip was sectioned, polished, etched with 5 mL of HNO₃ and 95 mL of methanol, and then observed under a scanning electron microscope (Joel: JCM-6000), as shown in Fig. 2. At the center of cross section, the microstructure is a combination between tempered sorbite and martensite, while evidence of decarburization is observed at the surface of cross section. The combination between tempered sorbite and martensite corresponds to the fact that e-clip requires high toughness. To increase the toughness, the martensite, i.e., the brittle phase occurs after quench hardening process, is transformed to softer phases by tempering process. At tempering temperature of 490–540 °C [9], the carbon atoms diffuse from martensite

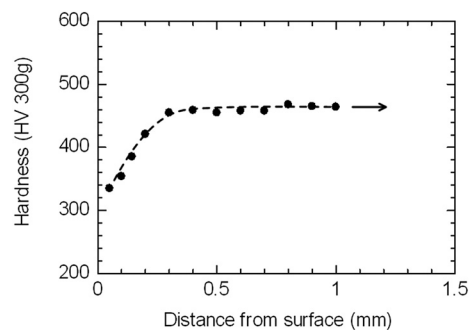


Fig. 3. Hardness profile on the cross section of e-clip.

to form a ferrite-cementite mixture or tempered sorbate, i.e., a phase with high toughness. At the location indicated by a dot on e-clip in Fig. 1, the hardness profile on the diameter line of e-clip is shown in Fig. 3. As a depth where the hardness becomes stable, the depth of decarburization is approximately 300 μm . Based on tensile testing, the stiffness of e-clip is 1.1 kN/mm.

2.2. Cyclic deformation

Cyclic deformation during fatigue experiment of e-clip was estimated using FEA. In the previous work [10], the cyclic deformation of e-clip was experimentally and numerically evaluated using railway track system with 15 base plates. Two wheel loads were compressed on an UIC60 rail [11]. The distance between wheels was 2100 mm, while the distance between base plates was 650 mm. The outer toe load was 1.07 kN, while the inner toe load was 1.03 kN. To simulate the curve rail, the lateral wheel load of 39 kN and vertical wheel load of 74 kN were applied on rail. These loads were suggested by AS 1085.19 [12] and BS EN 13481 [13] for curve rail of 20-ton axle load vehicle at speed of 100 km/h. Schematic illustrations of railway track system are shown in Fig. 4a.

Schematic illustrations of e-clip deformation are shown in Fig. 4b, where d_0 is the distance from the upper surface of base plate to the e-clip before installation, F_1 and d_1 are the toe load and distance from the upper surface of base plate to the e-clip after installation, and F_2 and d_2 are the toe load and distance from the upper surface of base plate to the e-clip under wheel loads. Because one e-clip is under the repeated wheel loads during actual operation; the cyclic deformation from d_1 to d_2 is likely to occur, i.e., $d_0 = 16.50$ mm, $d_1 = 27.15$ mm and $d_2 = 26.65$ mm. If the magnitude of deformation and number of cycles are high enough, the fatigue failure of e-clip is possible.

To obtain a broad analysis, the toe loads under 3 installation conditions were evaluated, i.e., low, normal, and high toe loads. The cyclic deformation for the fatigue experiment under normal toe load (i.e., normal e-clip installation) was obtained from the previous work [10], i.e., $d_0 = 16.50$ mm, $d_1 = 27.15$ mm and $d_2 = 26.65$ mm. However, the e-clip may be under-deformed or over-deformed during installations. To simulate the low toe load (i.e., under-deformed e-clip installation), the deformation of 2 mm was subtracted from the deformations of e-clip under normal installation (d_1 and d_2), while the deformation of 2 mm was added to the deformations of e-clip under normal installation (d_1 and d_2) to simulate the high toe load (i.e., over-deformed e-clip installation). Moreover, the impact causes by irregularities of rail and wheel, e.g., weldment, wear, corrugated rail, can add up to 60% of the wheel load [4,5]. To simulate the influence of impact on cyclic deformation, 60% of deformation was added to the cyclic deformation range (d_1-d_2), while the deformation under toe load (d_1) was unaltered. The deformations of e-clips under the influences of toe load and impact are summarized in Table 2. These cyclic deformations were used for the fatigue experiments of e-clips.

2.3. Fatigue experiment

Experimental set-up for the fatigue of e-clip is shown in Fig. 5. Two e-clips were clamped between the insulators and base plate with the rail and rail pad in the middle. The von Mises strains on e-clip were measured using a rosette strain gage (TML: FRA-5-11). The strain gage measurement had a precision of 0.5 μm . The location of strain measurement is shown in Fig. 1. The von Mises strain was multiplied by the modulus of e-clip to obtain the von Mises stress (σ_v), i.e., Hook's law. Subsequently, the von Mises stress was used for the validation of FEA.

Sinusoidal cyclic deformation with 5-Hz frequency was applied to the e-clips through a rail by a servo-hydraulic actuator (MTS: 244.22 with 100-kN load cell). A linear-variable differential transformers (LVDT) with 0.05-mm precision was used to control the deformation of e-clip. The cyclic deformations used for the fatigue experiments of e-clips are summarized in Table 2. The temperature and relative humidity during the fatigue experiment were controlled at $30 \pm 2^\circ\text{C}$ and $60 \pm 5\%$, respectively. The fatigue life is defined as the number of cycles that occur before complete fracture. However, if an e-clip does not fail after 5×10^6 cycles, it is considered as a run-out. To investigate the location of fatigue crack nucleation, the fracture surface of failed e-clip was observed using a scanning electron microscope (Joel: JCM-6000). The initiation and propagation of fatigue crack were evaluated, and the failure mechanism was discussed.

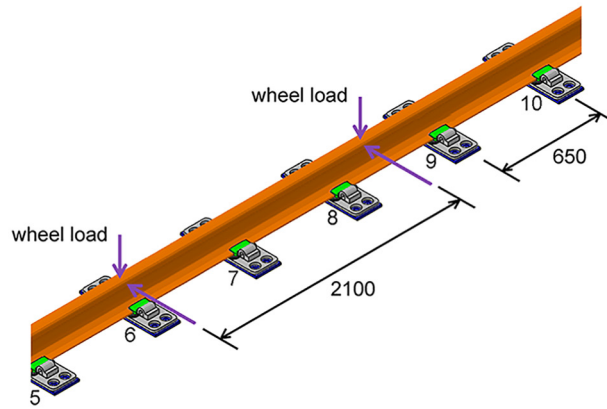
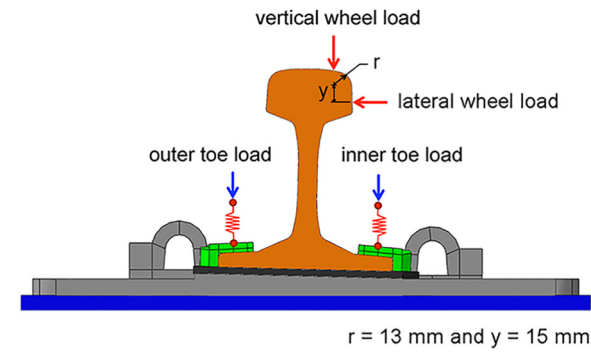
2.4. Finite element analysis

Stress distribution on e-clip was numerically evaluated using 3D linear-elastic FEA, i.e., ABAQUS [14]. FEA model, which composed of e-clip and base plate, is shown in Fig. 6. The elements of e-clip were 10-node tetrahedral elements, while those of rail, base plate and insulators were 8-node linear brick elements. The e-clip and base plate were made of steel, while the insulator was made of polymer [1,13]. The moduli of e-clip and base plate are 210 GPa, while their Poisson's ratios (ν) are 0.3. On the other hand, the modulus of insulator is 23 GPa, while its Poisson's ratio (ν) is 0.45. Frictional-contact elements, master-slave algorithm, and penalty method were applied to the contact interfaces. The slip of the contact interface was assumed to occur when the shear stress is greater than the critical shear stress (τ_c), i.e.,

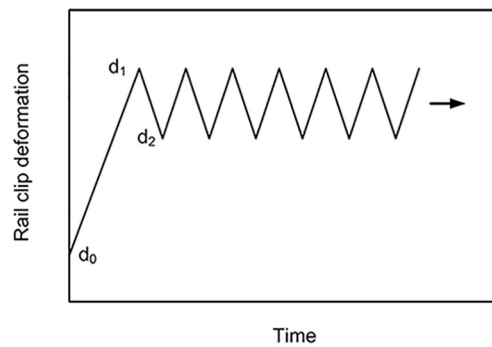
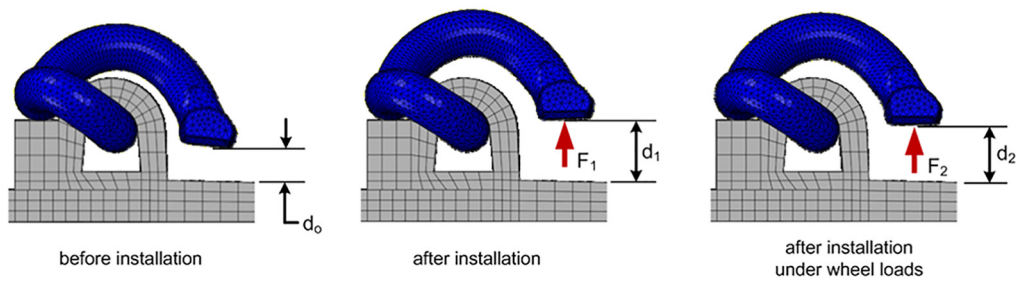
$$\tau \geq \tau_c = \mu \sigma_n \quad (1)$$

where σ_n and μ are the normal stress and the friction coefficient, respectively. The friction coefficient of 0.3 was assumed for all contacts. The boundary conditions were applied at the bottom of base plate. The displacements in all directions and the rotations around all axes were constrained.

Deformation of rail was gradually increased with intervals of 40 steps from zero to the maximum deformation. Subsequently, the deformation of e-clip, resistance force of e-clip and von Mises stress (σ_v) on e-clip were numerically calculated. To minimize the



(a)



(b)

Fig. 4. Schematic illustrations of; (a) railway track system (showing base plate no. 5–10), and (b) e-clip deformation (dimension in mm) [10].

Table 2
Cyclic deformations of e-clips.

E-clip deformation		d_1 (mm)	d_2 (mm)
Wheel load	Toe load		
Normal	Normal	27.15	26.65
	High	29.15	28.65
	Low	25.15	24.65
Impact	Normal	27.15	26.35
	High	29.15	28.35
	Low	25.15	24.35

Note: $d_o = 16.50$ mm for all cases of fatigue experiment.

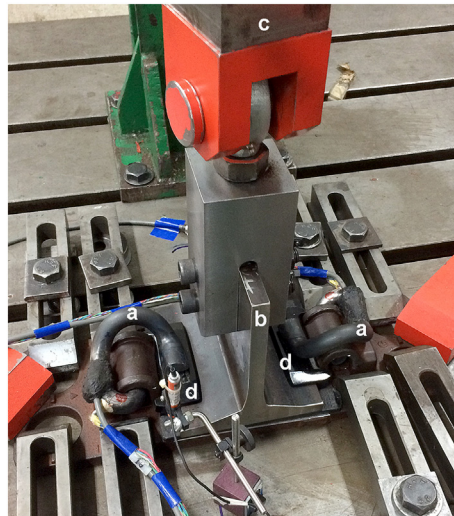


Fig. 5. Experimental set-up for the fatigue of e-clip (a – e-clips, b – rail, c – actuator, and d - insulators).

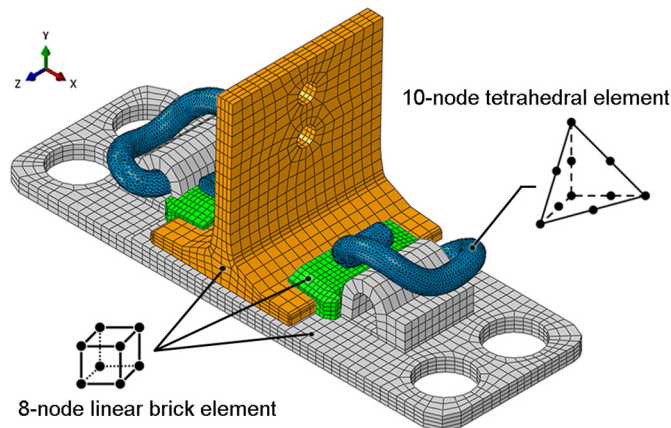


Fig. 6. FEA model of e-clip.

influence of element size, the size of elements was adjusted until the variation of the calculated resistance forces was below 5%. The numbers of elements of each FEA model are shown in Fig. 7a. Relationships between applied deformation (d_1-d_o) and resistance force of e-clips are shown in Fig. 7b. At 8-mm applied deformation, the resistance forces of FEA models with various numbers of elements are shown in Fig. 7c. The resistance force decreases with the increase in number of elements, and becomes stable at 37,491 elements (model B). As a ratio between the resistance force and deformation of e-clip, the stiffness of e-clips with 37,491 elements is estimated to be 1.1 kN/mm, which corresponds to that from the tensile testing. Therefore, the e-clip model with 37,491 elements was used in the present work.

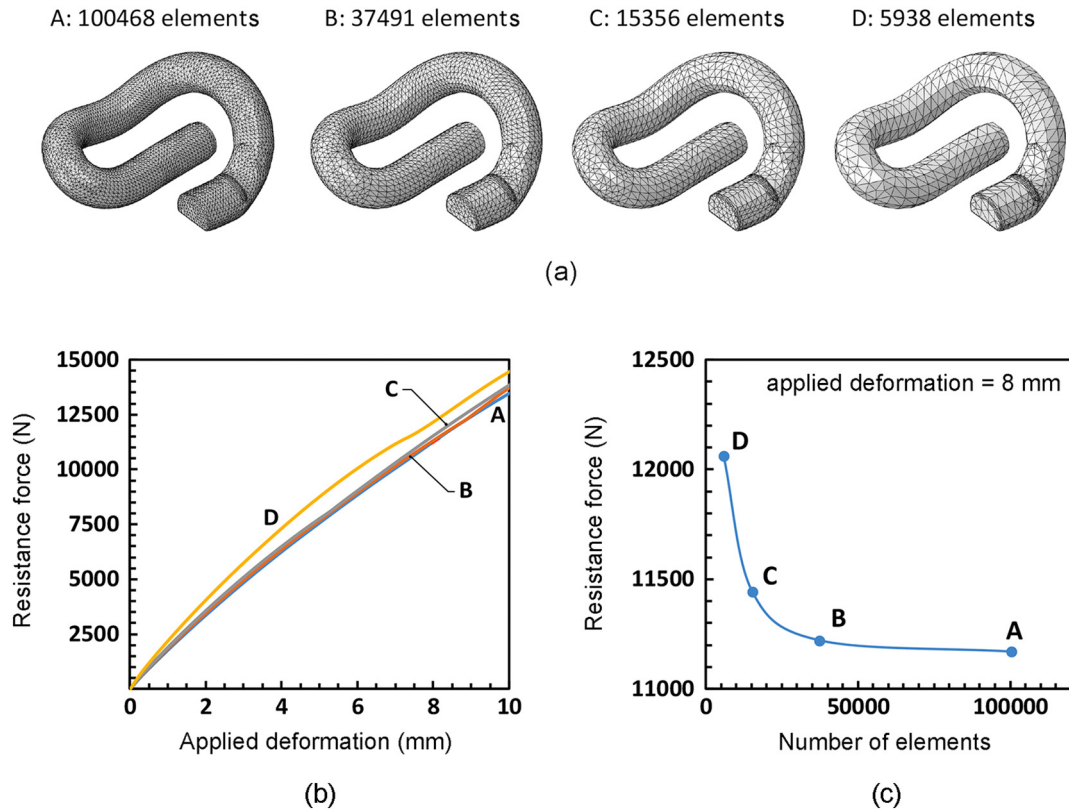


Fig. 7. (a) E-clip models with various numbers of elements, (b) resistance force vs. applied deformation, and (c) resistance forces at 8-mm applied deformation.

3. Results and discussion

3.1. Stress distribution

Under the 8.65-mm applied deformation (d_1-d_o), i.e. an approximated deformation of e-clip after under-deformed installation (low toe load), the distribution of von Mises stress on the surface of e-clip was calculated using FEA, as shown in Fig. 8a. The maximum von Mises stress on e-clip, i.e., the critical location of e-clip, was found near the location of strain gage (Fig. 1). At the critical location, the stresses in a function of applied deformation from experiment and FEA are compared in Fig. 8b. Because a rosette strain gage has the gage length of 3 mm, the calculated von Mises stresses under the gage area of rosette strain gage were averaged before the comparison. The experimental stresses are in good agreement with the stresses from FEA, i.e. the differences are lower than 5%. Therefore, the validation of FEA was confirmed. It is noted that the actual location and magnitude of the maximum stress of e-clip could not be accurately detected by strain gages, thus they should be numerically determined using FEA.

3.2. Fatigue life

Experimental results are summarized in Table 3. Under normal wheel load, the toe load had no influence on fatigue resistance of the e-clip, i.e., the e-clips with high, normal and low toe loads were run-out. However, with the contribution of impact, the fatigue lives were significantly reduced to 5468 cycles and 16,839 cycles for the e-clips with high and normal toe loads, respectively. Under low toe load with impact, the e-clip could withstand $> 5 \times 10^6$ cycles. During fatigue experiments, it was observed that the cracks were nucleated at the critical location of e-clips (Fig. 8a). Von Mises stresses at the critical location during fatigue experiments are summarized in Table 3.

Akiniwa et al. [15] have performed fatigue tests under reversed cyclic stresses using smooth specimens of an oil-tempered Si-Cr spring steel, which its chemical composition is listed in Table 1. The relationship between stress amplitude and fatigue life could be approximated by linear lines in double-logarithmic plots. They found that the stress amplitude of reversed cyclic loading at run-out ($N_f > 5 \times 10^6$ cycles) is approximately 800 MPa, while the yield stress and ultimate tensile stress are approximately 1200 MPa and 1500 MPa, respectively. Because the plain fatigue result (smooth specimens under reversed cyclic stresses) of the present spring steel is not available, the stress amplitude of reversed cyclic loading at 5×10^6 cycles and the ultimate tensile stress of a spring steel [15] were used for the fatigue evaluation of the e-clip. The mean stresses and stress amplitudes of the present fatigue experiments were

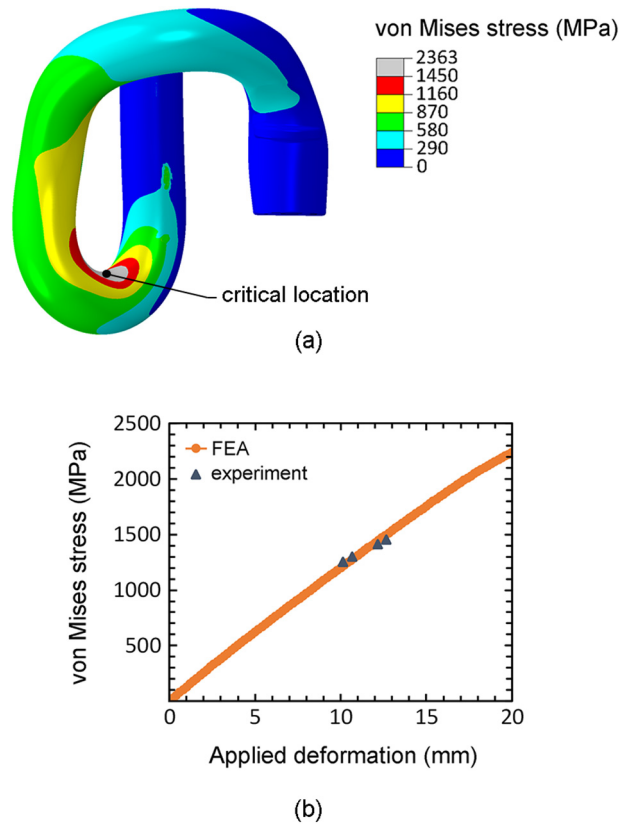


Fig. 8. (a) Distribution of von Mises stress at 8.65-mm applied deformation, and (b) von Mises stress at critical location vs. applied deformation.

Table 3
Von Mises stresses and fatigue lives on e-clips.

Clip deformation		σ_v at d_1 (MPa)	σ_v at d_2 (MPa)	Fatigue life (cycle)
Wheel load	Toe load			
Normal	Normal	1268	1230	$> 5 \times 10^6$
	High	1450	1412	$> 5 \times 10^6$
	Low	1041	1003	$> 5 \times 10^6$
Impact	Normal	1268	738	16,839
	High	1450	920	5468
	Low	1041	511	$> 5 \times 10^6$

Note: $\sigma_v = 0$ at d_0 .

plotted on the Goodman diagram [16],

$$\frac{\sigma_a}{\sigma_{ar}} + \frac{\sigma_m}{\sigma_u} = 1 \tag{2}$$

$$\sigma_u = \frac{\sigma_{max} - \sigma_{min}}{2} \tag{3}$$

$$\sigma_m = \frac{\sigma_{max} + \sigma_{min}}{2} \tag{4}$$

where, σ_{ar} is the stress amplitude of reversed cyclic loading, σ_a is the stress amplitude, σ_m is the mean stress, σ_u is the ultimate tensile stress, σ_{max} is the maximum stress or the σ_v at d_1 , and σ_{min} is the minimum stress or the σ_v at d_2 . Both σ_{max} and σ_{min} are summarized in Table 3.

Fatigue results correspond to the Goodman diagram, i.e., the mean stresses and stress amplitudes of run-out e-clips are under the line of Goodman equation, while those of failed e-clips are on and above the line of Goodman equation (Fig. 9). Therefore, the Goodman diagram can be used for the fatigue evaluation of the e-clip. It is noted that the tensile tests and plain fatigue tests of the present spring steel would provide more accurate Goodman diagram and fatigue evaluation of e-clip.

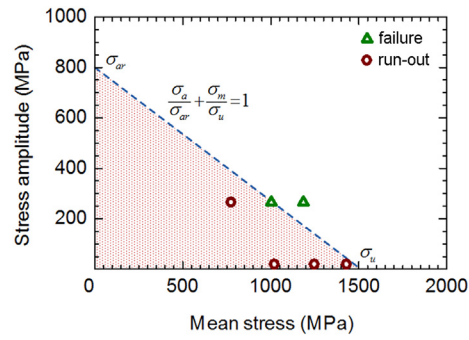


Fig. 9. Mean stress vs. stress amplitude.

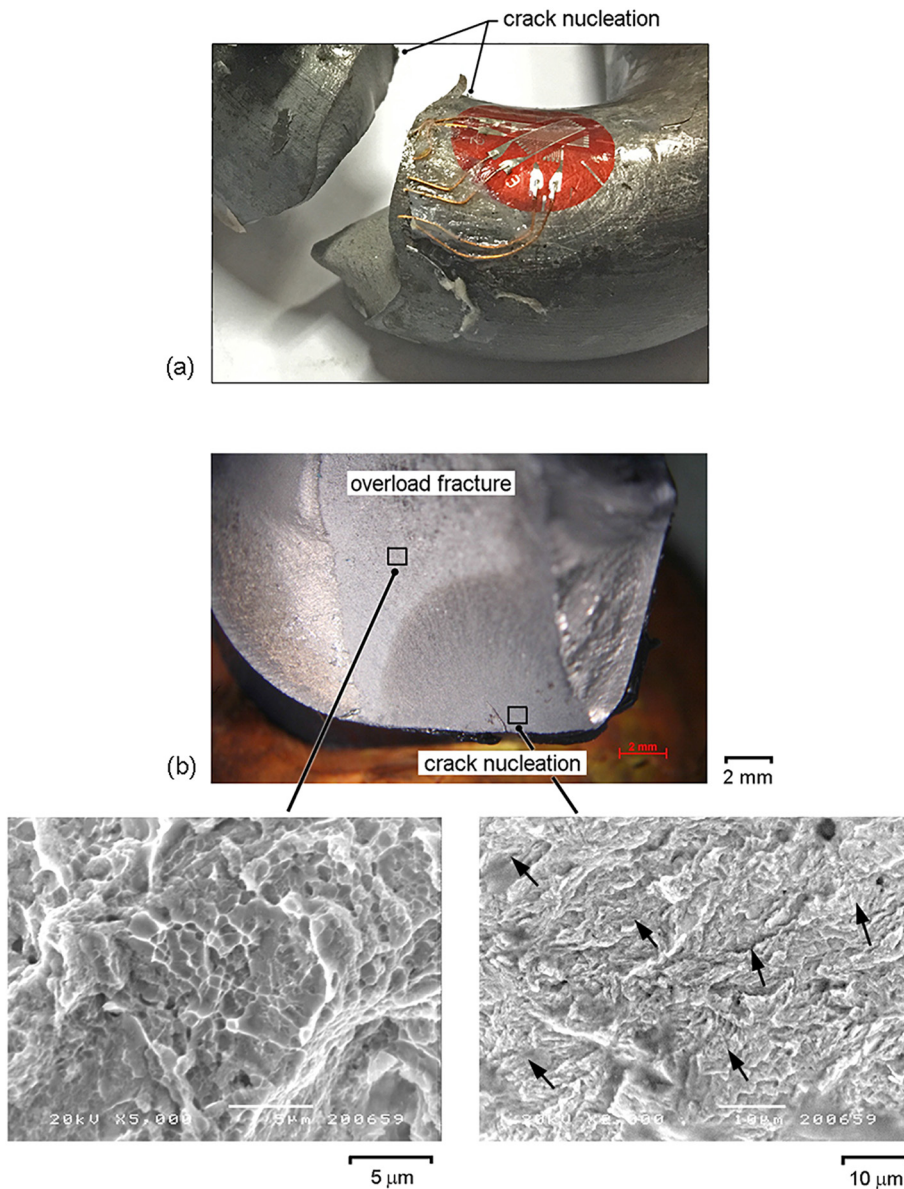


Fig. 10. E-clip under normal toe load and impact wheel load; (a) failed e-clip, and (b) fracture surface.

3.3. Fracture surface

After fatigue experiments, the failed e-clips were observed under a scanning electron microscope. The similar failure characteristic was observed on e-clip under normal toe load/impact wheel load, and e-clip under high toe load/impact wheel load. As an example, the failed e-clip and its fracture surface are shown in Fig. 10. The fatigue crack was found to nucleate at the location of highest stress, i.e., a critical location (Fig. 10a). After nucleation, the fatigue crack propagates into the e-clip, as indicated by arrows in Fig. 10b. The severity at fatigue crack front increases with the crack length until the overload fracture occurs. Severe plastic deformation or dimples were observed on entire region of overload fracture (Fig. 10b).

3.4. Recommendation

- Proper maintenance of railway track system is crucial to keep impact as low as possible. If all maintenances are appropriately carried out but the fatigue is still prevalent. A proposed solution based on these results is to reduce the toe load, as it showed the positive effect on the fatigue resistance of the e-clip under impact.
- Modifications in design should be taken into the consideration. The radius of curvature at the critical location should be increased to minimize the stress, while maintained the proper stiffness.
- Surface modification and/or heat treatment, which enhance the fatigue resistance, should be introduced into the production of e-clip. For example, the level of decarburization at the surface of e-clip should be minimized.

4. Conclusions

- Stresses and deformations calculated using FEAs were in good agreement with those of experiments. However, the actual location and magnitude of the maximum stress of e-clip could not be accurately detected by strain gages. Thus, they should be numerically determined using FEA.
- Toe load had no influence on fatigue resistance of e-clip under normal wheel load, i.e., the e-clips with high, normal, and low toe load were run-out after 5×10^6 cycles. However, under the contribution of impact, the fatigue lives were significantly reduced to 5468 cycles and 16,839 cycles for the e-clips with high and normal toe loads, respectively. Under low toe load with impact, the e-clip could withstand $> 5 \times 10^6$ cycles.
- Fatigue results corresponded to the Goodman diagram, i.e., the mean stresses and stress amplitudes of run-out e-clips were under the line of Goodman equation, while those of failed e-clips were on and above the line of Goodman equation. Therefore, the Goodman diagram could be used for the fatigue evaluation of the e-clip.
- Fatigue crack was found to nucleate at the location of highest stress. After nucleation, the fatigue crack propagated into the e-clip. The severity at fatigue crack front increased with the crack length until the overload fracture.

Acknowledgement

The authors would like to acknowledge the supports from Dr. Anchalee Manonukul (National Metal and Materials Technology Center, Thailand), the Thammasat University Research Fund, the Thailand Commission on Higher Education of Thailand (the National Research University Project), the Royal Golden Jubilee Ph.D. Program (RGJ), the Thailand Research Fund (TRF), and the National Research Council of Thailand (NRCT).

References

- [1] C. Esveld, *Modern Railway Track*, MRT-Productions, Netherlands, 2001.
- [2] C. Esveld, Recent developments in slab track, *Eur. Rail. Rev.* 2 (2003) 81–85.
- [3] S. Suresh, *Fatigue of Materials*, 2nd ed., Cambridge University Press, Cambridge, 1998.
- [4] L. Ling, W. Li, H. Shang, X. Xiao, Z. Wen, X. Jin, P. Augustin, Experimental and numerical investigation of the effect of rail corrugation on the behaviour of rail fastenings, *Veh. Syst. Dyn.* 52 (2014) 1211–1231.
- [5] S. Mohammadzadeh, S. Ahadi, M. Nouri, Stress-based fatigue reliability analysis of the rail fastening spring clip under traffic loads, *Lat. Am. J. Solids Struct.* 11 (2014) 993–1011.
- [6] S. Tamagawa, H. Kataoka, T. Deshimaru, A fatigue limit diagram for plastic rail clips, *WIT Trans. Built Envir.* 135 (2014) 839–848.
- [7] J. Sadeghi, M. Fesharaki, A. Khajehdezfuly, Influences of train speed and axle loads on life cycle of rail fastening clips, *Trans. Can. Soc. Mech. Eng.* 39 (2015) 1–11.
- [8] H.X. Shang, Z.F. Wen, L. Wu, W. Li, S.F. Zhang, X.S. Jin, Finite element analysis of type iii rail fastening clip failure in metro lines, *Gongcheng Lixue/Eng. Mech.* 32 (2015) 210–215.
- [9] JIS G 4801, Spring steels, The Japan Iron and Steel Federation, 2011.
- [10] A. Hasap, P. Paitekul, N. Noraphaiphaksa, C. Kanchanomai, Influence of toe load on fatigue failure of elastic rail clip, *J. Rail Rapid Transit* 232 (2018) 1078–1087.
- [11] BS EN 13674-1, Railway applications - Track - Vignole railway rails 46 kg/m and above, British-Adopted European Standard, 2002.
- [12] AS1085.19, Railway track material, The Australian Standard, Standards Australia International Ltd, Sydney, Australia, 2003.
- [13] BS EN 13481-2, Railway applications - Track - performance requirements for fastening systems. Fastening systems for concrete sleepers, British-Adopted European Standard, 2012.
- [14] ABAQUS User's Manual, ABAQUS Inc, 2016.
- [15] Y. Akiniwa, S. Stanzl-Tschegg, H. Mayer, M. Wakita, K. Tanaka, Fatigue strength of spring steel under axial and torsional loading in the very high cycle regime, *Int. J. Fatigue* 30 (2008) 2057–2063.
- [16] J. Goodman, *Mechanics Applied to Engineering*, Longman, Green & Company, London, 1899.